© 2017. Published by The Company of Biologists Ltd | Journal of Cell Science (2017) 130, 360-371 doi:10.1242/jcs.194191

RESEARCH ARTICLE

# Diverting CERT-mediated ceramide transport to mitochondria triggers Bax-dependent apoptosis

**Amrita Jain[1], Oliver Beutel[1,2], Katharina Ebell[1], Sergey Korneev[1] and Joost C. M. Holthuis[1,3,*]**

## ABSTRACT

A deregulation of ceramide biosynthesis in the endoplasmic reticulum (ER) is frequently linked to induction of mitochondrial apoptosis. Although *in vitro* studies suggest that ceramides might initiate cell death by acting directly on mitochondria, their actual contribution to the apoptotic response in living cells is unclear. Here, we have analyzed the consequences of targeting the biosynthetic flow of ceramides to mitochondria using a ceramide transfer protein (encoded by *COL4A3BP*) equipped with an OMM anchor, mitoCERT. Cells expressing mitoCERT import ceramides into mitochondria and undergo Bax-dependent apoptosis. Apoptosis induction by mitoCERT was abolished through (i) removal of its ceramide transfer domain, (ii) disruption of its interaction with VAMP-associated proteins (VAPs) in the ER, (iii) addition of antagonistic CERT inhibitor HPA12, (iv) blocking *de novo* ceramide synthesis and (v) targeting of a bacterial ceramidase to mitochondria. Our data provide the first demonstration that translocation of ER ceramides to mitochondria specifically commits cells to death and establish mitoCERT as a valuable new tool to unravel the molecular principles underlying ceramide-mediated apoptosis.

**KEY WORDS: Bcl-2 proteins, Ceramide transfer protein, Cytochrome *c*, Endoplasmic reticulum, Membrane contact sites, Mitochondrial apoptosis, VAP receptor**

## INTRODUCTION

Apoptosis is a form of programmed cell death with a crucial role in organismal development and tissue homeostasis. Perturbations in apoptosis contribute to human diseases including cancer and autoimmunity. The role of mitochondria in apoptosis that is triggered by diverse stress stimuli (e.g. DNA damage, cytokines) has been well established and provides an attractive target of therapeutic interventions (Czabotar et al., 2014; Tait and Green, 2013). Permeabilization of the mitochondrial outer membrane (MOM), allowing passage of intermembrane space proteins such as cytochrome *c*, is considered a point of no return in the suicide program, leading to activation of caspases that execute an ordered cellular self-destruction. MOM permeabilization (MOMP) is controlled by the B-cell lymphoma 2 (Bcl-2) protein family, which includes pro- and anti-apoptotic members that collectively determine the balance between cell death and survival (Luna-Vargas and Chipuk, 2016; Moldoveanu et al., 2014). The principal function of the anti-apoptotic Bcl-2 proteins is to antagonize the pro-apoptotic activities of the Bcl-2 proteins Bax and Bak (also known as BAK1), which are thought to directly engage in MOMP by creating proteolipid pores responsible for cytochrome *c* release (Kuwana et al., 2002; Salvador-Gallego et al., 2016; Wei et al., 2001).

Although apoptosis research has primarily focused on the role of Bcl-2 proteins, a growing body of evidence supports a crucial role for lipids. Notably, ceramides – central intermediates of sphingolipid metabolism – have frequently been implicated as potential mediators of mitochondrial apoptosis (Hannun and Obeid, 2008; Patwardhan et al., 2016). Numerous studies have revealed that cellular ceramide levels rise concomitantly with apoptosis induction in response to a variety of apoptotic stimuli, including tumor necrosis factor α (TNFα) (García-Ruiz et al., 2003; Luberto et al., 2002), chemotherapeutic agents (Alphonse et al., 2004; Bose et al., 1995) and radiation (Deng et al., 2008; Mesicek et al., 2010), through activation of sphingomyelinases, stimulation of *de novo* ceramide synthesis, or both. Interventions that suppress ceramide accumulation render cells resistant to these apoptotic stimuli, indicating that ceramides are necessary and sufficient to trigger mitochondrial apoptosis. Consequently, the potential of ceramide-based therapeutics in the treatment of cancer has become a major focus of interest. However, where and how ceramides exert their apoptogenic activity in cells is not well understood.

Some reports indicate that ceramides can promote apoptotic cell death by inhibiting phosphoinositide-3 kinase (PI3K) and Akt/PKB signaling, resulting in dephosphorylation and subsequent activation of the pro-apoptotic Bcl-2-family protein Bad (Bourbon et al., 2002; Zhu et al., 2011). Short-chain ceramides can activate protein phosphatase 2A (PP2A), which dephosphorylates and inactivates the anti-apoptotic protein BCL2 (Dobrowsky et al., 1993; Mukhopadhyay et al., 2009). An upregulation of ceramide levels has also been reported to sensitize cells to endoplasmic reticulum (ER) stress and promote activation of apoptotic regulators of the unfolded protein response (Liu et al., 2014; Park et al., 2008; Senkal et al., 2011; Swanton et al., 2007). Other studies have revealed that ceramides can form pores in planar membranes as well as in the outer membrane of isolated mitochondria that are large enough to allow passage of cytochrome *c* (Siskind et al., 2002, 2006). Interestingly, members of the anti-apoptotic Bcl-2 protein family prevent ceramide-induced permeabilization of isolated mitochondria, whereas a combination of pro-apoptotic Bax and ceramides enhances permeabilization (Ganesan et al., 2010; Siskind et al., 2008). This indicates that ceramides can act directly on mitochondria to promote MOMP and trigger apoptotic cell death. In line with this idea, mitochondrial targeting of a bacterial sphingomyelinase to generate ceramides in mitochondria induces cytochrome *c* release and apoptosis (Birbes et al., 2001). Moreover, ER-like membranes associated with isolated mitochondria appear to

[1]Molecular Cell Biology Division, Department of Biology/Chemistry, University of Osnabrück, Osnabrück D-49076, Germany. [2]Max-Planck-Institute for Molecular Cell Biology and Genetics, Dresden D-01307, Germany. [3]Membrane Biochemistry & Biophysics, Bijvoet Center and Institute of Biomembranes, Utrecht University, Utrecht 3584 CH, The Netherlands.

*Author for correspondence (holthuis@uos.de)

K.E., 0000-0001-9800-2781; J.C.M.H., 0000-0001-8912-1586

**Received 23 June 2016; Accepted 14 November 2016**

Journal of Cell Science (2017) 130, 360-371 doi:10.1242/jcs.194191

produce enough ceramides to allow transient penetration of the outer membrane by pro-apoptotic proteins (Stiban et al., 2008). However, the actual contribution of mitochondrial ceramides to the apoptotic response in living cells is a topic of controversy (Ségui et al., 2006; Wang et al., 2009; Chipuk et al., 2012). Resolving this issue is challenging because ceramides are readily metabolized into various other bioactive lipid species, which can influence the sensitivity of cells to apoptosis through multiple pathways (Hait et al., 2006; Hannun and Obeid, 2008). Moreover, apoptotic stimuli such as TNFα trigger ceramide accumulation in multiple organelles (Birbes et al., 2005; Dbaibo et al., 2001; Luberto et al., 2002).

Ceramides are synthesized *de novo* through N-acylation of sphingoid bases, a reaction that is catalyzed by ceramide synthases on the cytosolic surface of the ER (Tidhar and Futerman, 2013). In mammals, the bulk of newly synthesized ceramides is converted to sphingomyelin by sphingomyelin synthase in the lumen of the trans-Golgi (Tafesse et al., 2006). Delivery of ER ceramides to the site of sphingomyelin production requires the cytosolic ceramide transfer protein CERT (encoded by *COL4A3BP*) (Hanada et al., 2003). Besides a ceramide transfer or START domain, CERT contains a pleckstrin homology domain that binds to phosphatidylinositol 4-monophosphate (PI4P) at the trans-Golgi and a FFAT motif that is recognized by the ER-resident VAMP-associated proteins A and B (VAP-A and VAP-B, respectively) (Kawano et al., 2006). CERT might operate within the narrow cytoplasmic gap at contact sites between the ER and trans-Golgi to establish efficient ceramide transport for sphingomyelin production. Mammalian cells contain two sphingomyelin synthase isoforms, namely SMS1 in the trans-Golgi and SMS2 at the plasma membrane (also known as SGMS1 and SGMS2, respectively) (Huitema et al., 2004; Yamaoka et al., 2004). Together with SMS-related protein SMSr (also known as SAMD8), they form the SMS family. SMSr is not a conventional sphingomyelin synthase but instead synthesizes trace amounts of the sphingomyelin analog ceramide phosphoethanolamine in the lumen of the ER (Vacaru et al., 2009). SMSr is the best-conserved member of the SMS family, with homologs in organisms that lack sphingomyelin (Vacaru et al., 2013). Unexpectedly, disrupting SMSr catalytic activity in mammalian cells causes an accumulation of ER ceramides and their mislocalization to mitochondria, triggering a mitochondrial pathway of apoptosis (Tafesse et al., 2014; Vacaru et al., 2009). Apoptosis induction is prevented by blocking *de novo* ceramide synthesis, stimulating ceramide export from the ER or targeting a bacterial ceramidase to mitochondria (Tafesse et al., 2014). These results imply that ER ceramides are authentic transducers of apoptosis and that their arrival in mitochondria is a critical step in committing cells to death.

In the present study, we verified the above concept by diverting CERT-mediated ceramide transport to mitochondria. This was accomplished by targeting CERT to the OMM while retaining its ability to interact with VAP proteins in the ER. We found that expression of mitoCERT triggers a mitochondrial pathway of apoptosis, as evidenced by cytosolic translocation of cytochrome *c* and activation of caspase 9. Apoptosis induction was abolished through the removal of Bax, required ongoing *de novo* ceramide biosynthesis and critically relied on the ability of mitoCERT to transport ceramides at ER–mitochondria junctions. These results indicate that ceramide delivery to mitochondria specifically induces apoptotic cell death, and they highlight a novel approach for probing the compartment-specific functions of ceramides as key determinants of cell fate.

## RESULTS

### Mitochondrial targeting of CERT

CERT targets the Golgi by recognizing PI4P through its N-terminal plextrin homology domain (Hanada et al., 2003). To direct CERT-mediated ceramide transport to mitochondria, the plextrin homology domain of CERT was swapped against the OMM (OMM) anchor sequence of mouse A-kinase anchor protein 1 (AKAP1), generating mitoCERT (Fig. 1A). A FLAG-tag was added to the C-terminus of CERT and mitoCERT to facilitate their detection. Contrary to CERT, mitoCERT expressed in human HeLa cells colocalized with a mitochondrial marker and was fully recovered from a membrane-bound fraction, indicating that the protein was efficiently targeted to mitochondria (Fig. 1B,C).

CERT contains a short peptide sequence or FFAT motif (consensus sequence EFFDAxE, where x is any amino acid), which interacts with the ER-resident tail-anchored proteins VAP-A and VAP-B (Kawano et al., 2006; Loewen et al., 2003). The interaction between CERT and VAPs is crucial for efficient ER-to-Golgi transfer of ceramide. Indeed, CERT carrying a mutation in its FFAT motif (D324A) loses the ability to bind VAPs and cannot transfer ceramide to the Golgi efficiently (Kawano et al., 2006). Therefore, we next investigated the ability of mitoCERT to interact with VAPs. When expressed in HeLa cells, VAP-A that had been fused to GFP displayed a reticular cytosolic distribution that was reminiscent of the ER (Fig. 2A). Upon co-expression with CERT, GFP-tagged VAP-A accumulated in the perinuclear region. This perinuclear localization of VAP-A was lost when co-expressed with a CERT-D324A point mutant, as reported previously (Kawano et al., 2006) (Fig. 2A). When co-expressed with mitoCERT, VAP-A showed a tubular distribution that largely coincided with the mitoCERT- and Tom20-positive mitochondrial network (Fig. 2A,B). In cells expressing mitoCERT with the D324A point mutation, VAP-A retained a reticular distribution throughout the cytosol that showed little overlap with the mitochondrial network (Fig. 2A,B). This indicates that mitochondria-localized mitoCERT is able to bind to VAP receptors in the ER.

### MitoCERT acts as a VAP-dependent ER–mitochondria tether

The ability of mitoCERT to interact with ER-resident VAP receptors suggests that the protein might influence the contact area between ER and mitochondria by acting as an inter-organellar tether. To address this possibility, we first monitored changes in ER–mitochondria contacts using rapamycin-inducible linkers based on the FKBP–FRB heterodimerization system (Csordás et al., 2010) (Fig. 3A). These linkers were tagged with photoconvertable fluorophores to allow visualization of ER–mitochondria contacts by super-resolution microscopy. Addition of rapamycin caused a rapid (within 10 min) expansion of ER–mitochondria contact sites in cells that expressed the linkers (Fig. 3B,F). Consistent with this finding, subcellular fractionation experiments revealed that ∼40% of the ER-resident protein calnexin was recovered from mitochondrial pellets prepared from rapamycin-treated cells, whereas no more than 5% of calnexin was recovered from mitochondrial pellets of control cells (Fig. 3C). In contrast, super-resolution fluorescence microscopy and subcellular fractionation experiments revealed that expression of mitoCERT did not lead to any obvious increase in the contact area between ER and mitochondria. However, in cells that overproduced VAP-A, mitoCERT expression caused a significant expansion of ER–mitochondria contact sites (Fig. 3D–F). Based on these results, we conclude that mitoCERT acts as a VAP-dependent ER–mitochondria tether.

Journal of Cell Science (2017) 130, 360-371 doi:10.1242/jcs.194191

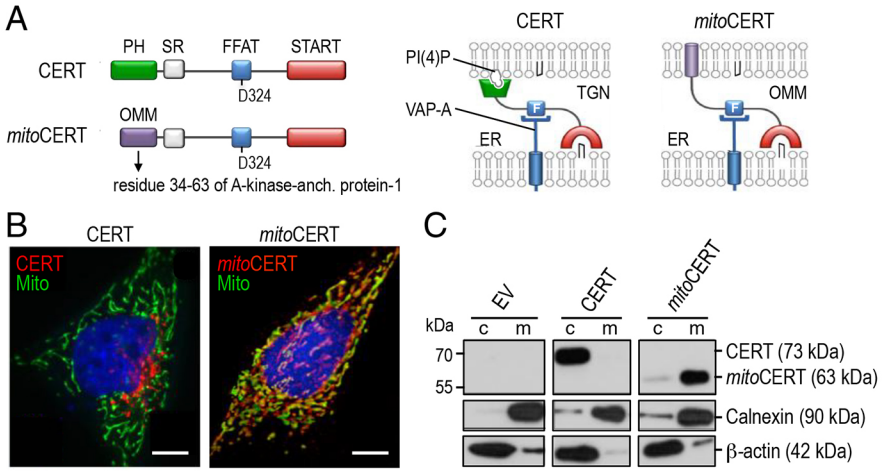


**Fig. 1. Mitochondrial targeting of ceramide transfer protein CERT.** (A) Schematic outline of CERT and mitoCERT. PH, pleckstrin homology domain; SR, serine-rich domain; FFAT, VAP-binding domain; START, ceramide-binding domain; PI(4)P, phosphatidylinositol-4-phosphate; TGN, trans-Golgi network; OMM, outer mitochondrial membrane. (B) MitoCERT localizes to mitochondria. HeLa cells that had been transfected with Flag-tagged CERT or mitoCERT were fixed, co-stained with antibodies against the Flag epitope (red) and mitochondrial protein p60 (Mito, green), and then visualized by fluorescence microscopy. (C) Contrary to CERT, mitoCERT co-fractionated with membranes. Immunoblots of cytosol (c) and total membranes (m) derived from HeLa cells that had been transfected as described in B were stained for the Flag epitope, calnexin and β-actin. EV, empty vector.

### MitoCERT mediates ceramide delivery to mitochondria

We next examined whether mitoCERT can mediate ceramide transfer to mitochondria. First, we analyzed the ability of the protein to bind to ceramide. To this end, lysates of mitoCERT-expressing HeLa cells were photoaffinity-labeled with pacCer, a bifunctional ceramide analog containing a photoactivatable diazirine and clickable alkyne group in its 15-carbon-long N-linked fatty acyl chain (Fig. 4A). Ultraviolet (UV) irradiation of the diazirine group generates a highly-reactive pacCer intermediate that can form a covalent linkage with proteins in its direct vicinity (Svenja Bockelmann, John Mina, Per Haberkant and J.C.M.H., unpublished data). Click chemistry is then used to decorate the alkyne group with a fluorophore, allowing visualization of the crosslinked protein–lipid complex by in-gel fluorescence. As proof-of-principle, lysates of HeLa cells expressing FLAG-tagged CERT were incubated with pacCer-containing liposomes and then

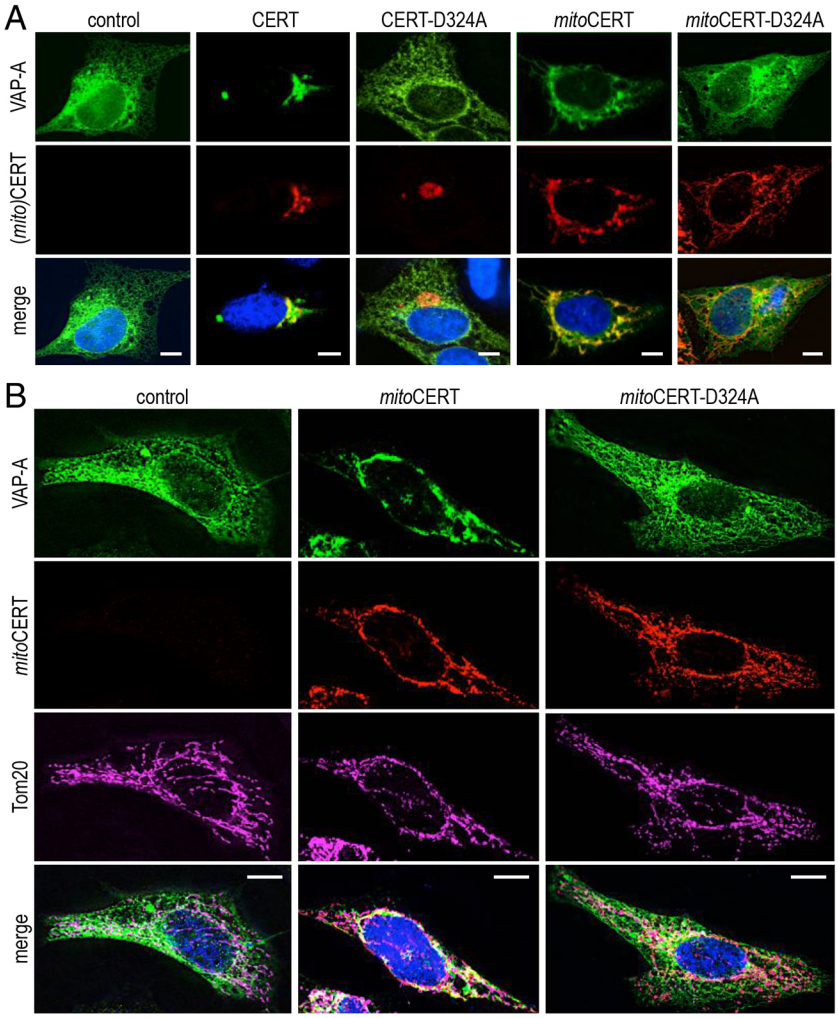


**Fig. 2. Mitochondria-localized mitoCERT interacts with VAP-A in the ER.** (A) HeLa cells that had been co-transfected with eGFP–VAP-A (green) and Flag-tagged CERT, mitoCERT or the VAP-A-binding mutants CERT-D324A and mitoCERT-D324A were fixed, stained with anti-Flag antibody (red) and then visualized by fluorescence microscopy. Scale bars: 10 µm. (B) HeLa cells that had been co-transfected with mCherry–VAP-A (green), Tom20–eGFP (magenta) and Flag-tagged mitoCERT or the VAP-A-binding mutant mitoCERT-D324A were fixed and stained with anti-Flag antibody (red) and then visualized by fluorescence microscopy. Scale bars: 10 µm.

Journal of Cell Science (2017) 130, 360-371 doi:10.1242/jcs.194191

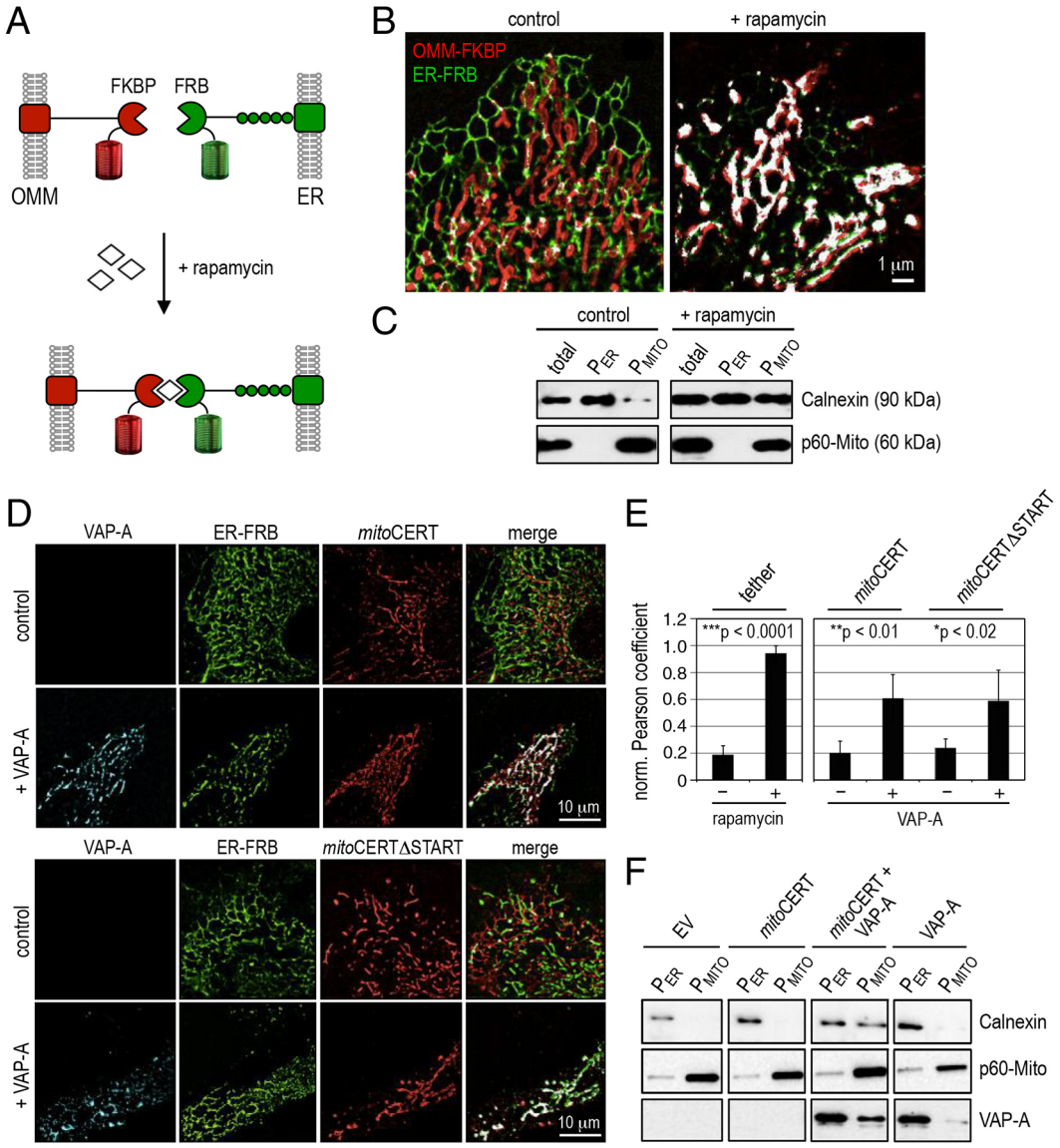


**Fig. 3. Impact of mitoCERT expression on contact sites between ER and mitochondria.** (A) Schematic of the rapamycin-inducible fluorescent ER–mitochondria linkers paGFP-ER-FRB and OMM-FKBP-HALO. (B) Fluorescence photoactivation localization microscopy (fPALM) and dStorm images showing ER (green) and mitochondrial networks (red) in HeLa cells that had been transfected with rapamycin-inducible ER–mitochondria linkers before (control) and after treatment with rapamycin (+rapamycin; 50 nM, 30 min). OMM-FKBP-HALO was conjugated to HTL-TMR. Note that contact areas between ER and mitochondria (white) expanded dramatically upon rapamycin treatment. (C) Subcellular fractionation analysis confirmed rapamycin-induced expansion of ER–mitochondria junctions. HeLa cells that had been transfected with rapamycin-inducible ER–mitochondria linkers were treated as described in B and then subjected to subcellular fractionation, yielding total membranes (total) and membrane fractions enriched for ER ($P_{ER}$) or mitochondria ($P_{MITO}$). Equal volumes of each fraction where analyzed by immunoblotting against markers for ER (calnexin) and mitochondria (P60-Mito). (D) MitoCERT acts as a VAP-dependent ER–mitochondria tether. fPALM and dStorm images of HeLa cells that had been co-transfected with the indicated combinations of HALO-ER-FRB (green), mitoCERT–Flag (red), mitoCERTΔSTART–Flag (red) and paGFP–VAP-A (cyan). Immunodetection of Flag-tagged proteins was with Cy5-conjugated rabbit polyclonal secondary antibody. Contact areas between ER and mitochondria (white) expanded substantially when mitoCERT or mitoCERTΔSTART were co-expressed with paGFP–VAP-A (+VAP-A). (E) Pearson correlation coefficients between ER and mitochondria determined in cells treated as described in B and D. The maximum correlation coefficient measured was set at 1. Data are mean±s.d. ($n$=3). ***$P$<0.0001; **$P$<0.01; *$P$<0.02, by two-tailed unpaired Student's $t$-test. (F) Subcellular fractionation analysis confirming mitoCERT-dependent expansion of ER–mitochondria junctions in VAP-A-overproducing cells. HeLa cells that had been transfected with Flag-tagged mitoCERT, mitoCERTΔSTART and/or paGFP–VAP-A were processed as described in C. Note that co-expression of paGFP–VAP-A and mitoCERT resulted in expanded ER–mitochondria contact sites, as evidenced by an enhanced recovery of ER-resident calnexin and paGFP–VAP-A (VAP-A) from mitochondrial membrane pellets. Immunoblots shown are representative of two independent experiments.

subjected to UV irradiation followed by a click reaction with Alexa-Fluor-647 azide. This approach yielded a fluorescent protein of 73 kDa that reacted with anti-FLAG antibodies and that was absent in pacCer-labeled lysates of control cells (Fig. 4B, left panel). Photoaffinity-labeled lysates of cells that expressed FLAG-tagged mitoCERT, by contrast, contained a fluorescent and immunoreactive protein of 63 kDa (Fig. 4B, right panel). Removal of the ceramide transfer or START domain yielded a 38-kDa protein, mitoCERTΔSTART, which failed to react with pacCer upon UV cross-linking. These data show that, analogous to CERT, mitoCERT is able to extract ceramide from a lipid bilayer through its START domain.

Journal of Cell Science (2017) 130, 360-371 doi:10.1242/jcs.194191

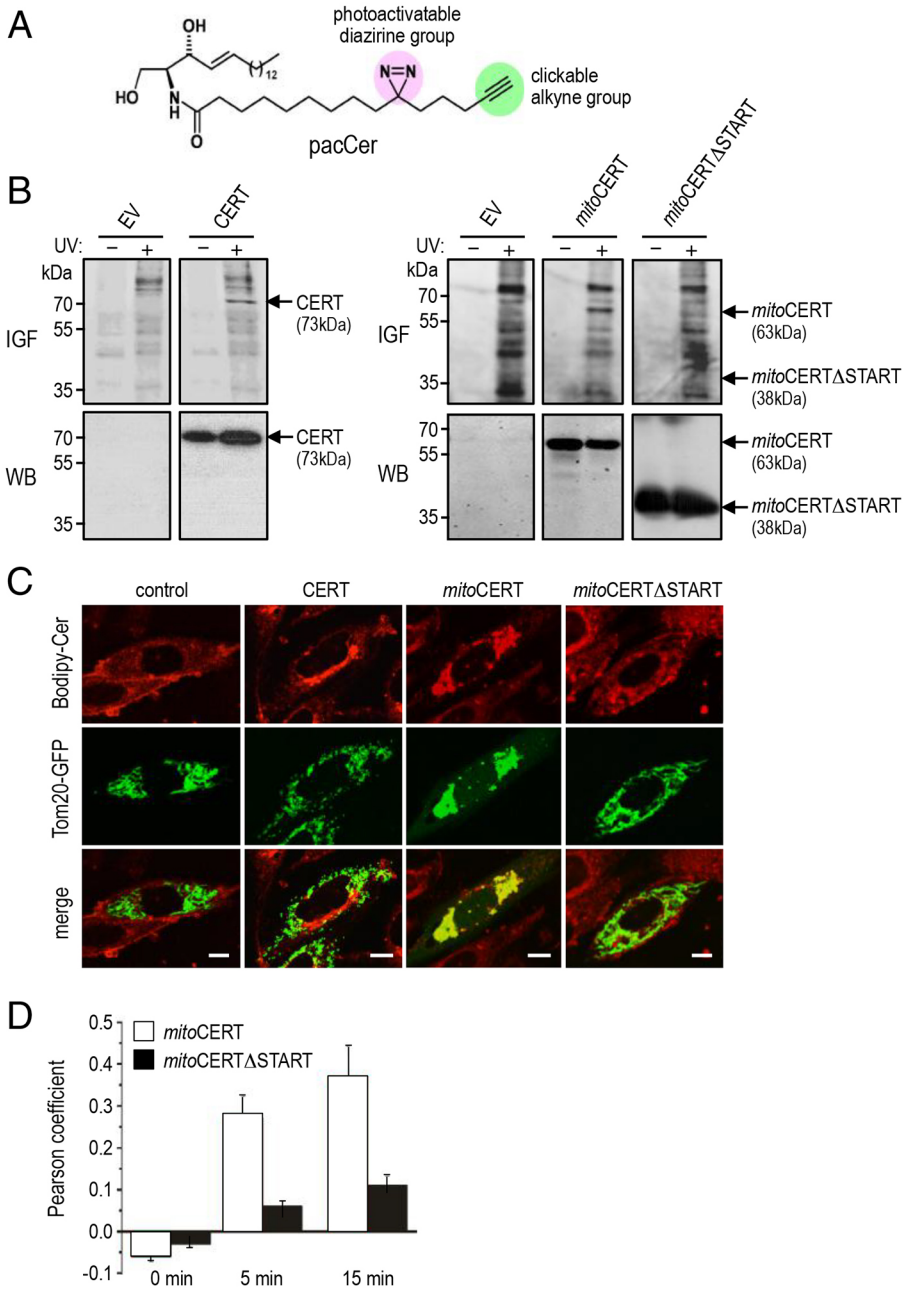


**Fig. 4. MitoCERT binds to ceramides and catalyzes their transport to mitochondria.** (A) Structure of the photoactivatable and clickable C15-ceramide analog, pacCer. (B) Photoaffinity labeling of mitoCERT with pacCer. Total lysates of HeLa cells expressing Flag-tagged CERT, mitoCERT or mitoCERTΔSTART were incubated with pacCer-containing liposomes for 30 min at 37°C, subjected to UV irradiation and then click-reacted with Alexa-Fluor-647 azide. Lysates were analyzed by in-gel fluorescence (top) or processed for immunoblotting using an anti-Flag antibody (bottom). (C) MitoCERT mediates delivery of C5-Bodipy–ceramide to mitochondria. CHO LY-A cells that had been co-transfected with the mitochondrial marker Tom20–GFP and empty vector (control), CERT, mitoCERT or mitoCERTΔSTART were incubated with 0.5 µM red fluorescent C5-Bodipy–ceramide at 4°C for 30 min, chased at 37°C for 15 min, and then visualized by confocal fluorescence microscopy. Scale bars: 10 µm. (D) Pearson correlation coefficients between C5-Bodipy–ceramide and mitochondria were determined in CHO LY-A cells that had been co-transfected with Tom20–GFP and mitoCERT or mitoCERTΔSTART. Cells were pulse-labeled with C5-Bodipy–ceramide at 4°C for 30 min and then chased for 0, 5 or 15 min at 37°C. Data are mean±s.d. (*n*=3).

We next addressed whether mitoCERT can mediate ceramide transport to mitochondria. To this end, the intracellular movement of a fluorescent analog of ceramide (C5-Bodipy–Cer) was monitored in Chinese hamster ovary (CHO) LY-A cells that had been transfected with GFP-tagged Tom20 as mitochondrial marker. In these cells, ER-to-Golgi transport of C5-Bodipy–Cer is disrupted owing to a loss-of-function mutation in the CERT-encoding gene (Hanada et al., 2003). In cells that expressed wild-type CERT, transport was restored and C5-Bodipy–Cer accumulated in the perinuclear Golgi region (Fig. 4C). However, in cells that expressed mitoCERT, C5-Bodipy–Cer was readily delivered to mitochondria. In contrast, cells expressing mitoCERTΔSTART failed to deliver C5-Bodipy–Cer to mitochondria (Fig. 4C,D). These results demonstrate that mitoCERT is able to bind to ceramides and can mediate their transport to mitochondria.

## MitoCERT triggers ceramide-dependent mitochondrial apoptosis

A rise in mitochondrial ceramide levels has been implicated in the activation of mitochondrial apoptosis (Birbes et al., 2001; Lee et al., 2011; Tafesse et al., 2014). Therefore, we next analyzed the ability of mitoCERT to trigger mitochondria-mediated cell death. Within 24 h after transfection, mitoCERT-expressing HeLa cells released cytochrome *c* into the cytosol (Fig. 5A) and displayed proteolytic activation of caspase 9 (Fig. 5B,C), two hallmarks of mitochondrial apoptosis that are also observed in staurosporine-treated cells. Moreover, mitoCERT expression led to cleavage of the caspase substrate PARP, membrane blebbing and cell death (Fig. 5B; data not shown). Treatment with the pan-caspase inhibitor z-VAD-fmk blocked cleavage of caspase 9 and PARP (Fig. 5D), and prevented membrane blebbing and cell death (data not shown), indicating that mitoCERT activates a caspase-dependent pathway of

Journal of Cell Science (2017) 130, 360-371 doi:10.1242/jcs.194191

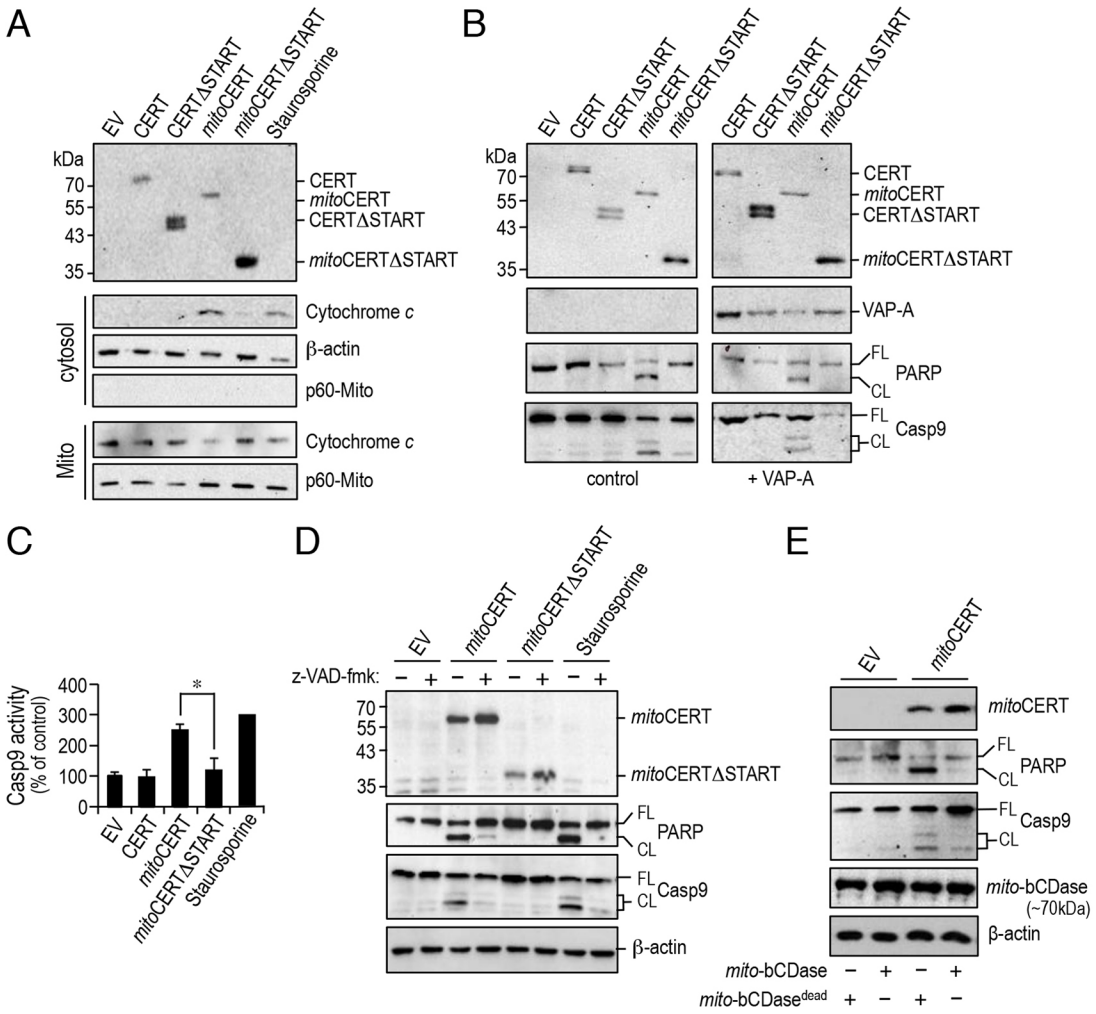


**Fig. 5. MitoCERT activates a ceramide-dependent pathway of mitochondrial apoptosis.** (A) MitoCERT expression triggers cytosolic release of cytochrome *c*. HeLa cells that had been treated with staurosporine (1 µM, 4 h) or transfected with empty vector (EV), Flag-tagged CERT, CERTΔSTART, mitoCERT or mitoCERTΔSTART (24 h) were lysed and subjected to subcellular fractionation. Total cell lysates, cytosol and mitochondrial pellets were processed for immunoblotting with antibodies against the Flag epitope (top), cytochrome *c*, β-actin and mitochondrial protein p60-Mito (bottom). Note that removal of the START domain abolished the ability of mitoCERT to induce translocation of cytochrome *c*. (B) MitoCERT expression induces cleavage of caspase 9 (Casp9) and PARP. HeLa cells that had been co-transfected with empty vector (control) or VAP-A–eGFP (+VAP-A) and Flag-tagged CERT, CERTΔSTART, mitoCERT or mitoCERTΔSTART were lysed and processed for immunoblotting with antibodies against the Flag epitope, eGFP (VAP-A), PARP and caspase 9. FL, full length; CL, cleaved. (C) Cells that had been treated as described in A were lysed and analyzed for caspase-9 activity using a colorimetric assay. Levels of caspase-9 activity were expressed relative to that in cells that had been transfected with empty vector (EV). Error bars indicate mean±s.d., $n$=3. *$P$<0.05 by two-tailed unpaired Student's $t$-test. (D) Pan-caspase inhibitor z-VAD-fmk blocks caspase-9 and PARP cleavage in mitoCERT-expressing cells. HeLa cells that had been treated as described in A were incubated in the absence (–) or presence (+) of z-VAD-fmk and then processed for immunoblotting. (E) Targeting a bacterial ceramidase to mitochondria abrogates apoptosis induction in mitoCERT-expressing cells. HeLa cells that had been co-transfected with empty vector (EV) or Flag-tagged mitoCERT and a catalytically active or dead bacterial ceramidase carrying a mitochondria-targeting signal and Myc tag (mito-bCDase, mito-bCDase$^{dead}$) were lysed and processed for immunoblotting with antibodies against PARP, caspase 9 and the Flag and Myc epitopes. Immunoblots shown are representative of two independent experiments.

apoptosis. In contrast, cells overproducing CERT or expressing mitoCERTΔSTART were devoid of any of the aforementioned apoptotic phenotypes (Fig. 5A–D). Although mitoCERTΔSTART was unable to bind to and transfer ceramides (Fig. 4), it retained the ability to act as a VAP-dependent ER–mitochondria tether (Fig. 3D,F). This implies that ER–mitochondria tethering is unlikely to represent the principal mechanism by which mitoCERT-expressing cells are committed to death. Indeed, expanding the contact area between ER and mitochondria through overproduction of VAP-A had no obvious impact on the fate of either mitoCERT- or mitoCERTΔSTART-expressing cells (Fig. 5B). Rather, the ability of mitoCERT to catalyze ceramide transport to mitochondria appeared to be important for its apoptogenic activity. To examine this further, we next used a *Mycobacterium*-derived ceramidase equipped with an N-terminal mitochondrial-targeting signal, mito-bCDase. We have previously demonstrated that heterologous expression of mito-bCDase effectively prevents ceramide accumulation in mitochondria of SMSr-depleted HeLa cells (Tafesse et al., 2014). When co-expressed with mito-bCDase, mitoCERT lost the ability to induce caspase-9 and PARP cleavage (Fig. 5E). This rescuing effect was abolished through mutation of two invariant histidine residues (His96 and His98) in the active site of mito-bCDase, indicating that a catalytically active form of the enzyme is required to prevent mitoCERT-mediated cell death. From

Journal of Cell Science (2017) 130, 360-371 doi:10.1242/jcs.194191

this, we conclude that the apoptogenic activity of mitoCERT crucially relies on its ability to deliver ceramides to mitochondria.

### The apoptogenic activity of mitoCERT relies on its interaction with VAP and requires *de novo* ceramide synthesis

As mitoCERT interacts with ER-resident VAPs, a likely source of the ceramides responsible for committing mitoCERT-expressing cells to death is the ER. To test this directly, we initially set out to monitor mitochondrial delivery of *de novo* synthesized ceramides through metabolic labeling of control and mitoCERT-expressing cells with [2,3,3-d3] serine ($D_3$-serine) followed by mass spectrometry quantification of $D_3$-serine-labeled ceramides in purified mitochondria. However, this approach did not yield a conclusive answer as $D_3$-serine-labeled ceramides were hard to detect and it was difficult to exclude their partial turnover during the time-consuming preparation of mitochondria that were free of ER and other contaminating organelles. Therefore, we next investigated the impact of blocking *de novo* ceramide synthesis on mitoCERT-induced cell death. Treatment with long chain base synthase inhibitor myriocin or ceramide synthase inhibitor fumonisin B1 in each case fully suppressed cleavage of caspase 9 and PARP in mitoCERT-expressing cells (Fig. 6A). Addition of HPA12, a specific inhibitor of CERT-mediated ceramide transport (Kumagai et al., 2005), also blocked caspase-9 and PARP cleavage in these cells. Collectively, these data support the idea that mitoCERT triggers apoptosis by transferring ceramides from the ER to mitochondria. As efficient ceramide trafficking from the ER to the Golgi is crucially dependent on the ability of CERT to interact with ER-resident VAPs (Kawano et al., 2006), we next analyzed VAP-binding mutant mitoCERT-D324A for its ability to induce apoptosis. Unlike mitoCERT, expression of mitoCERT-D324A failed to trigger cleavage of caspase 3, caspase 9 and PARP in HeLa cells (Fig. 6B–D). These results indicate that the ceramides responsible for activating mitochondrial apoptosis in mitoCERT-expressing cells primarily originate from the ER.

### MitoCERT-induced apoptosis is crucially dependent on Bax but not Bak

Besides HeLa cells, several other human cancer cell lines proved to be susceptible to mitoCERT-induced apoptosis. These included ovarium carcinoma OVCAR3 and SKOV1, non-small lung carcinoma A549, and colon carcinoma HCT116 cells. In all cases examined, removal of the START domain or substitution of Ala for Asp at position 324 in the FFAT motif abolished mitoCERT-mediated apoptogenic activity (Fig. 7A). These results indicate that diverting CERT-mediated ceramide trafficking to mitochondria is sufficient to commit cells to death and that this process is not restricted to one particular cell type. It has been proposed that ceramides can trigger apoptosis by forming channels in the OMM to allow passage of cytochrome *c* (Siskind et al., 2002, 2006). However, other models postulate that ceramide-mediated apoptosis relies on participation of the pro-apoptotic Bcl-2 proteins Bax and Bak (Beverly et al., 2013; Chipuk et al., 2012; von Haefen et al., 2002). This led us to examine the consequences of Bax and Bak removal on mitoCERT-induced apoptosis in HCT116 cells. Treatment with staurosporine served as control. Loss of Bak had no measurable impact on caspase-9 or PARP cleavage in either mitoCERT-expressing or staurosporine-treated cells (Fig. 7B). In contrast, removal of Bax essentially abolished caspase-9 and PARP cleavage in both mitoCERT-expressing and staurosporine-treated cells. MitoCERT expression caused, at best, only some residual PARP cleavage in Bax-deficient cells. The apoptogenic activity of mitoCERT was completely eliminated in Bak- and Bax-deficient

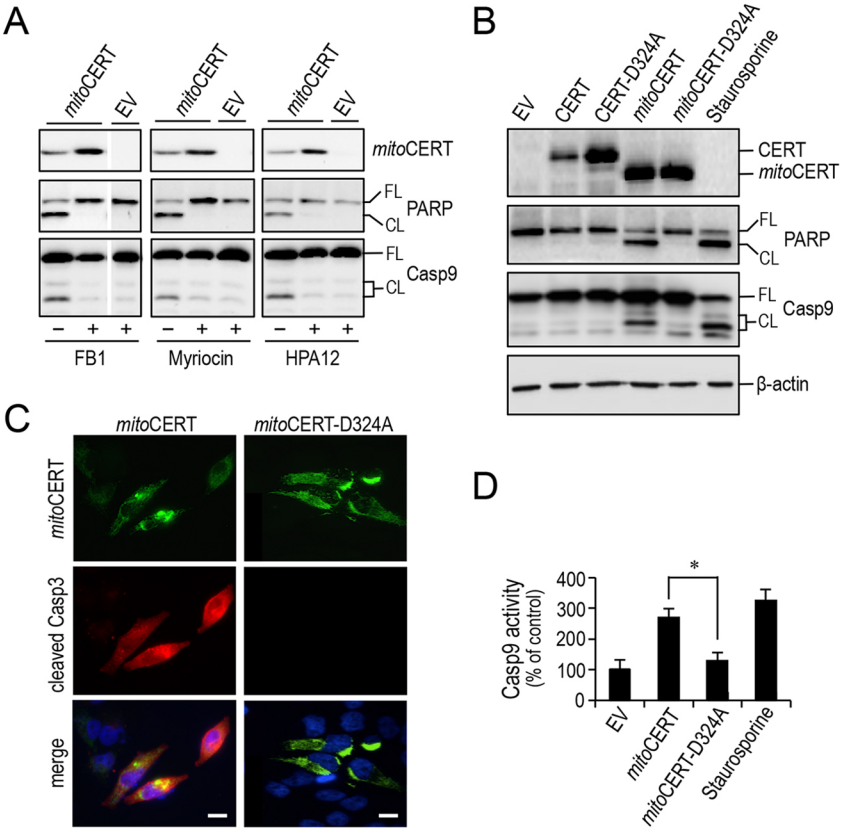


**Fig. 6. Apoptogenic activity of mitoCERT relies on its interaction with VAP and is sensitive to inhibitors of *de novo* ceramide synthesis.** (A) HeLa cells that had been transfected with empty vector (EV) or Flag-tagged mitoCERT were treated with inhibitors of long-chain base synthase (myriocin, 30 µM), ceramide synthase (fuminosin FB1, 25 µM) or CERT (HPA12, 10 µM), lysed and processed for immunoblotting with antibodies against the Flag epitope, PARP and caspase 9 (Casp9). (B) HeLa cells that had been transfected with empty vector (EV) or Flag-tagged CERT, mitoCERT or the VAP-binding mutants CERT-D324A or mitoCERT-D324A were lysed and processed for immunoblotting with antibodies against the Flag epitope, PARP, caspase 9 and β-actin. (C) HeLa cells that had been transfected with Flag-tagged mitoCERT or mitoCERT-D324A were fixed, co-stained with DAPI (blue) and antibodies against the Flag epitope (green) or cleaved caspase 3 (red; Casp3) and then visualized by fluorescence microscopy. Scale bars: 20 µm. (D) Cells that had been treated as described in B were lysed and analyzed for caspase-9 activity with a colorimetric assay. Levels of caspase-9 (Casp9) activity were expressed relative to those in cells that had been transfected with empty vector (EV). Error bars indicate mean±s.d., $n$=3. *$P$<0.05 by two-tailed unpaired Student's $t$-test. FL, full length; CL, cleaved.

Journal of Cell Science (2017) 130, 360-371 doi:10.1242/jcs.194191

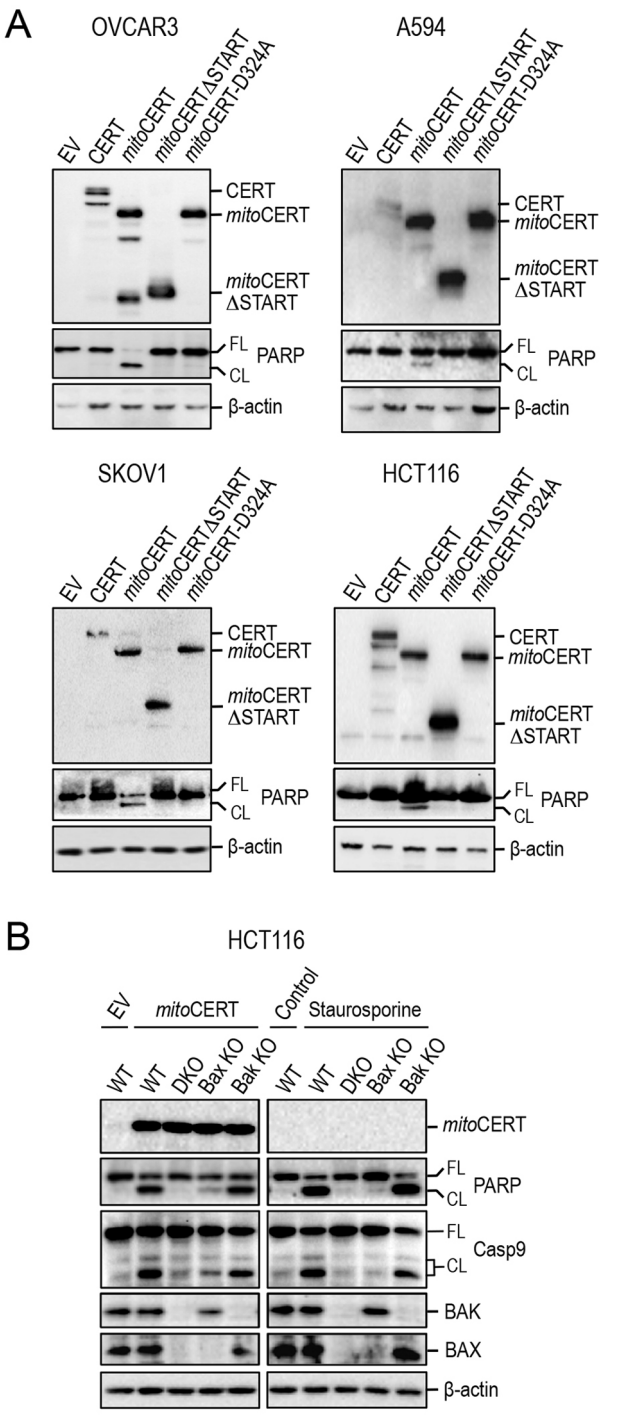


**Fig. 7. MitoCERT-induced apoptosis is largely independent of cell type and crucially relies on the pro-apoptotic Bcl-2 protein Bax.** (A) Human ovarium carcinoma OVCAR3 cells, ovarium carcinoma SKOV1 cells, non-small lung carcinoma A549 cells and colon carcinoma HCT116 cells were transfected with empty vector (EV) or Flag-tagged versions of CERT, mitoCERT, mitoCERTΔSTART or mitoCERT-D324A. At 24 h post-transfection, cells were processed for immunoblotting with antibodies against the Flag epitope, PARP and β-actin. FL, full length; CL, cleaved. (B) Wild-type (WT), $Bax^{-/-}$ (Bax KO), $Bak^{-/-}$ (Bak KO) and $Bax^{-/-}Bak^{-/-}$ (DKO) HCT116 cells were treated with staurosporine (1 µM, 4 h) or transfected with empty vector (EV) or Flag-tagged mitoCERT. At 24 h post transfection, cells were processed for immunoblotting with antibodies against the Flag epitope, PARP, caspase 9 (Casp9), Bak, Bax and β-actin. Note that removal of Bax virtually abolished mitoCERT-induced PARP and caspase-9 cleavage. Immunoblots shown are representative of three independent experiments.

cells. From this, we conclude that activation of mitochondrial apoptosis by mitoCERT primarily relies on Bax, analogous to the apoptotic pathway activated in staurosporine-treated HCT116 cells (Wang and Youle, 2012).

## DISCUSSION

Ceramides are widely believed to be authentic transducers of apoptosis, but how these biomolecules help commit cells to death is not well understood. A deregulation of ceramide levels in the ER has frequently been linked to induction of mitochondrial apoptosis. Although some reports indicate that ceramides influence this process by sensitizing cells to ER stress and activating apoptotic regulators of the unfolded protein response, experiments with isolated mitochondria suggest that ceramides are able to initiate the execution phase of apoptosis by directly promoting MOMP. To better define where and how ceramides exert their apoptogenic activity in cells, we here analyzed the consequences of targeting the biosynthetic ceramide flow to mitochondria using a ceramide transfer protein equipped with an OMM anchor, mitoCERT. We show that mitoCERT expression activates a ceramide-mediated mitochondrial pathway of apoptosis that requires the pro-apoptotic Bcl-2 protein Bax. Our findings provide a direct demonstration that translocation of ER ceramides to mitochondria suffices to commit cells to death, hence highlighting subcellular topology as a key determinant in ceramide-induced apoptosis.

Complementary lines of evidence indicate that apoptosis induction in mitoCERT-expressing cells is due to the arrival of ER ceramides in the mitochondria. To begin with, the apoptogenic activity of mitoCERT required an intact ceramide transfer or START domain and was crucially dependent on the ability of the mitochondria-anchored protein to bind to VAP receptors in the ER. The latter observation raised the possibility that mitoCERT triggers apoptosis by tightening the contact area between the ER and mitochondria, which has previously been reported to make mitochondria prone to $Ca^{2+}$ overloading, resulting in MOMP and apoptotic cell death (Csordás et al., 2010, 2006). However, mitoCERT-mediated tethering between ER and mitochondria, although required, was not sufficient to initiate mitochondrial apoptosis given that removal of the START domain abolished the apoptogenic activity of mitoCERT without compromising its ER–mitochondria tethering activity. In addition, overproduction of VAP-A in either mitoCERT- or mitoCERTΔSTART-expressing cells greatly expanded the contact area between ER and mitochondria without having any impact on cell fate. Moreover, mitoCERT-induced apoptosis was effectively blocked by HPA12, an antagonistic inhibitor of CERT-mediated ceramide trafficking (Kudo et al., 2010; Kumagai et al., 2005). Thus, a ceramide transfer-competent form of mitoCERT capable of bridging the cytoplasmic gap between mitochondria and ER proved critical for apoptosis induction. Blocking *de novo* ceramide production by pharmacological inhibitors of ceramide or long chain base synthases abrogated apoptosis induction in mitoCERT-expressing cells, indicating that mitochondrial delivery of ER ceramides by mitoCERT is responsible for triggering cell death. Indeed, targeting a catalytically active bacterial ceramidase to mitochondria fully suppressed mitoCERT-induced cell death.

Our current work complements and extends previous *in vitro* studies indicating that ceramides can act directly on mitochondria to promote MOMP and trigger apoptotic cell death. So how do ceramides help accomplish the release of pro-apoptotic proteins from the mitochondrial intermembrane space? Recent biochemical experiments with purified mitochondria have revealed that ceramides can influence mitochondrial integrity indirectly,

Journal of Cell Science (2017) 130, 360-371 doi:10.1242/jcs.194191

namely as precursors of two other molecules, sphingosine-1-$PO_4$ (S1P) and hexadecenal, which co-operate specifically with Bak and Bax to promote MOMP (Chipuk et al., 2012). Activation of these functionally related proteins involves a displacement of helix α1, leading to distal exposure of their BH3 domains. Binding of S1P to Bak and hexadecenal to Bax might lower the thermodynamic constraints on these conformational changes, thus facilitating their assembly into proteolipid pores that mediate the release of cytochrome *c*. This implies that ceramides, upon arrival in mitochondria, are metabolically converted into S1P and hexadecenal through the consecutive actions of three distinct enzymes: ceramidase, sphingosine kinase and S1P lyase (Chipuk et al., 2012). However, we here show that mitochondrial targeting of a bacterial ceramidase prevents apoptosis in mitoCERT-expressing cells, arguing that apoptogenic activity relies on intact ceramides rather than the downstream metabolic intermediates of ceramide turnover. Other studies have revealed that Bak can influence ceramide-induced apoptosis by acting as a positive regulator of *de novo* ceramide synthesis, a function unrelated to its pore-forming activity (Siskind et al., 2010). Thus, ceramides arriving in mitochondria might dissociate Bak from anti-apoptotic Bcl-2 proteins, thereby increasing the concentration of Bak available to activate ceramide synthases and establishing a feed-forward loop to promote apoptosis (Beverly et al., 2013). As removal of Bak had no influence on mitoCERT-induced apoptosis, it appears unlikely that an upregulation of *de novo* ceramide synthesis is part of the mechanism by which mitoCERT commits cells to death.

Another model is based on the observation that ceramides can form stable channels in planar lipid bilayers as well as in the outer membrane of purified mitochondria that are large enough to allow passage of cytochrome *c* (Siskind et al., 2002, 2006). Formation of ceramide channels does not require any auxiliary proteins but is disrupted by anti-apoptotic Bcl2 proteins (Chang et al., 2015; Siskind et al., 2008). Thus, the pore-forming activity of ceramides has been put forward as a potential mechanism for releasing pro-apoptotic proteins during the induction phase of apoptosis (Colombini, 2016). However, our finding that mitoCERT-induced apoptosis requires Bax is hard to reconcile with the idea that MOMP in mitoCERT-expressing cells relies exclusively on self-assembly of ceramides into channels. One possibility compatible with our data is that the pore-forming activity of ceramides synergizes with that of Bax to induce MOMP and initiate end-stage apoptosis. Indeed, experiments performed on mitochondria that had been isolated from rat liver or yeast indicated that, at concentrations at which externally added ceramides and Bax have little effect on their own, the combination induces substantial MOMP (Ganesan et al., 2010). Other studies have revealed that ceramides accumulating in the mitochondrial membrane of mammalian cells upon irradiation might form platforms into which Bax inserts, oligomerizes and functions as a pore (Lee et al., 2011). Interestingly, ceramides have a profound impact on membrane curvature (Trajkovic et al., 2008), and mitochondrial shape has been shown to govern Bax-mediated MOMP and apoptosis (Renault et al., 2015). Thus, rather than acting as autonomous apoptotic factors per se, ceramides might primarily serve to enhance mitochondrial Bax insertion and its functionalization into a proteolipid pore. Whether this process relies on direct and specific interactions between Bax and ceramides, mitochondria-associated ceramide effector proteins and/or ceramide-induced alterations in membrane curvature remains to be established.

So far, most studies addressing ceramide-activated cell death pathways rely on the application of cell-permeable (truncated) ceramides or the treatment of cells with apoptotic stimuli that influence ceramide pools in multiple organelles. Because lipid-mediated pathways typically operate at the level of individual organelles, such approaches make it hard to de-convolute the sequence of events through which ceramides commit cells to death. Experiments with isolated organelles, by contrast, require validation in intact cells. Application of mitoCERT bypasses a number of drawbacks associated with the above methods, thus providing a novel opportunity to unravel compartment-specific mechanisms that govern ceramide-mediated apoptotic cell death.

## MATERIALS AND METHODS

### Reagents

Staurosporine, myriocin, rapamycin and glucose oxidase were purchased from Sigma-Aldrich and catalase from Roche Applied Science. z-VAD-fmk was from Calbiochem and fumonisin B1 was obtained from Cayman Chemicals. Bodipy-TR-labeled C5-ceramide (Bodipy–Cer) and Alexa-Fluor-647 azide were from Thermo Fischer Scientific. 1,2-dioleoyl-sn-glycero-3-phosphocholine (DOPC) and 1,2-dioleoyl-sn-glycero-3-phosphoethanolamine (DOPE) were from Avanti Polar Lipids. D-erythro-sphingosine was purchased from Enzo Biochem.

### Synthesis of pacCer and HPA12

A 15-carbon (C15)-long fatty acid containing a photoactivatable diazerine and clickable alkyne group, pacFA, was synthesized in three steps from commercially available educts as described previously (Haberkant et al., 2013). Next, pacFA was coupled to D-erythro-sphingosine using a combination of 1-ethyl-3-(3-dimethylaminopropyl)carbodiimide (EDCI) and hydroxybenzotriazole (HOBT) as condensing reagents, yielding the photoactivatable and clickable C15-ceramide analog, pacCer (Svenja Bockelmann, John Mina, Per Haberkant and J.C.M.H., unpublished data). CERT inhibitor HPA12 was generated in nine steps from available educts with a total yield of 13% as described previously (Ďuriš et al., 2011), with the following modifications. We found that catalytic hydrogenative de-protection of the amino-function in the intermediate (1-phenylethylamino) diole caused removal of the benzylic hydroxyl group. Complementary protection of all hydroxyl groups in the form of tert-butyldimethylsilyl (TBDMS) ethers enabled us to avoid this undesirable reduction during the hydrogenation step. Further acylation of the free amine with lauric acid (DCC/DMAP) followed by hydrolytic desilylation (TBAF) resulted in the formation of HPA12 with satisfactory total yield. All synthetic compounds were purified to a high degree (>99%), and their structures were confirmed by $^{1}H$ and $^{13}C$ nuclear magnetic resonance and electrospray-ionization mass spectrometry (ESI MS) analyses.

### Antibodies

The following antibodies were used: mouse monoclonal anti-β-actin (cat. no. A1978, 1:10.000; Sigma-Aldrich), rabbit polyclonal anti-FLAG (cat. no. 2368, 1:1000; Cell Signaling), rabbit monoclonal anti-Bak (cat. no. 12105, 1:1000; Cell Signaling), rabbit monoclonal anti-Bax (cat. no. 5023, 1:1000; Cell Signaling), rabbit polyclonal anti-cleaved caspase-3 (cat. no. 9661, 1:200; Cell Signaling) and rabbit polyclonal anti-caspase-9 (cat. no. 9502, 1:700; Cell Signaling), mouse monoclonal anti-cytochrome *c* (sc13156, 1:500; Santa Cruz), mouse monoclonal anti-PARP-1 (sc8007, 1:1000; Santa Cruz), rabbit polyclonal anti-Myc (sc789, 1:700; Santa Cruz) and rabbit polyclonal anti-calnexin (sc11397, 1:1000; Santa Cruz), mouse monoclonal anti-mitochondrial surface protein p60 (cat. no. MAB1273, 1:1000; Millipore) and rabbit polyclonal anti-GFP (cat. no. NB600-303, 1:5000; Novus Biologicals) antibodies. Goat anti-mouse (cat. no. 31430, 1:10.000) and goat anti-rabbit IgG conjugated to horseradish peroxidase (cat. no. 31460, 1:10.000) were from Thermo Fischer Scientific. Cy™-dye-conjugated donkey anti-mouse and donkey anti-rabbit antibodies (cat. no. 715-225-150, 715-225-152, 715-165-150, 715-165-152, 715-175-150 and 715-175-152, 1:400 each) were from Jackson ImmunoResearch Laboratories.

### DNA constructs

A DNA insert encoding human CERT with a C-terminal FLAG tag (DYKDDDDK) was created by PCR and inserted into *Not*I and *Xba*I

Journal of Cell Science (2017) 130, 360-371 doi:10.1242/jcs.194191

restriction sites of mammalian expression vector pcDNA3.1 (+). MitoCERT was created by substituting the first 117 N-terminal residues of CERT for the OMM anchor sequence of mouse AKAP1 (V84389, residues 34–63: MAIQLRSLFPLALPGLLALLGWWWFFSRKK). Deletion of their START domains (residues 346–597) yielded CERTΔSTART and mitoCERTΔSTART. VAP-binding-deficient mutants CERT-D324A and mitoCERT-D324A were created using site-directed mutagenesis. Ectopic expression of fluorescent proteins was performed using mammalian expression vector pSEMS (Covalys Biosciences) containing monomeric eGFP (meGFP), photoactivatable GFP (paGFP) or HaloTag (HALO) (Wilmes et al., 2015). A cDNA encoding human VAP-A (kindly provided by Neale Ridgway, Dalhousie University, Halifax, Canada) was PCR amplified and inserted into pSEMS-mCherry, pSEMS-meGFP or pSEMS-paGFP in *Xho*I and *Sac*I restriction sites, creating mCherry–VAP-A, meGFP–VAP-A and paGFP–VAP-A, respectively. Constructs encoding the rapamycin-inducible fluorescent ER-mitochondria linkers paGFP-FRB-ER (Sac1), HALO-FRB-ER(Sac1) and OMM(Akap1)-FKBP-HALO were created by inserting the relevant domains from constructs CFP-FRB-ER (Sac1) and OMM(Akap1)-FKBP-RFP (Csordás et al., 2010) (kindly provided by György Hajnóczky, Thomas Jefferson University, Philadelphia) into pSEMS-paGFP and pSEMS-HALO expression vectors into *Xho*I and *Sac*II or *Eco*RV and *Eco*RI restriction sites. Constructs encoding mitochondrially targeted and catalytically active or dead bacterial ceramidase (mito-bCDase and mito-bCDaseH96A-H98A, respectively) have been described previously (Tafesse et al., 2014). Tom20–eGFP was a kind gift from Karin Busch, University of Osnabrück, Germany.

### Cell culture and transfection

Unless indicated otherwise, all cell lines used in this study were obtained from the American Type Culture Collection (ATCC) and routinely tested for mycoplasma contamination. HeLa (ATCC-CCL2), SKOV1 (kindly provided by Toon de Kroon, University of Utrecht, the Netherlands) and A594 cells (ATCC-CCL185) were cultured in high-glucose Dulbecco's modified Eagle's medium (DMEM) supplemented with 2 mM L-glutamine and 10% FBS. OVCAR3 cells (ATCC-HTB161) were cultured in RPMI with 10% FBS and CHO-LYA cells in Ham's F12 minimal essential medium with 10% FBS. HCT116 (ATCC-CCL247), HCT116-Bax$^{-/-}$, HCT116-Bak$^{-/-}$ and HCT116-Bax$^{-/-}$Bak$^{-/-}$ cells (kindly provided by Richard Youle, National Institute of Health, Bethesda, MD) were cultured in McCoy's medium with 10% FBS. Cells were transfected with DNA constructs using Effectene (Qiagen) according to the manufacturer's protocol. Fuminosin B1 (25 µM), myriocin (30 µM) and HPA12 (10 µM) were added immediately after transfection. Staurosporine (1 µM) was added 4–5 h before cell harvest. Both adherent and non-adherent cells were harvested 24 h post-transfection, washed twice in ice-cold 0.25 M sucrose and homogenized in ice-cold IM buffer (5 mM Hepes-KOH, pH 7.0, 250 mM mannitol, 0.5 mM EGTA, 1 mM protease inhibitor cocktail, 0.1 mM phenylmethanesulfonyl fluoride) by flushing through a Balch homogenizer 20–30 times using a 2-ml syringe as described previously (Tafesse et al., 2014). Cell homogenates were centrifuged twice at 600 $g_{max}$ for 5 min at 4°C to remove nuclei. The protein concentration of post-nuclear supernatants was determined by using a Bradford assay (Bio-Rad). Post-nuclear supernatants were normalized for total protein content before immunoblot analysis. Caspase-9 enzyme activity levels were determined using a colorometric assay kit (Biovision) following the manufacturer's protocol.

### Subcellular fractionation

Post-nuclear supernatants were centrifuged at 9000 $g_{max}$ for 10 min at 4°C to pellet mitochondria. Mitochondrial pellets were washed in ice-cold IM buffer and centrifuged twice (9000 $g_{max}$ for 10 min, 4°C) to remove contaminating ER. The post-mitochondrial supernatant was centrifuged again at 9000 $g_{max}$ for 10 min at 4°C to remove contaminating mitochondria and at 100,000 $g_{max}$ for 1 h at 4°C to pellet microsomal membranes. The post-microsomal supernatant (cytosolic fraction) was collected, and the microsomal pellet was washed once in IM buffer and centrifuged again (100,000 $g_{max}$ for 60 min, 4°C) to remove contaminating cytosol. Mitochondrial and microsomal pellets were resuspended in Buffer R (10 mM Tris-HCl, pH 7.4, 0.25 M sucrose, 1 mM protease inhibitor cocktail, 0.1 mM PMSF) before immunoblot analysis using organelle-specific antibodies.

### Photoaffinity labeling

Unilamellar liposomes containing pacCer were prepared from a defined lipid mixture (DOPC:DOPE:pacCer, 80:20:1 mol%) in $CHCl_3$:MeOH (9:1, v:v) using a mini-extruder (Avanti Polar Lipids). In brief, 10 µmol of total lipid was dried in a Rotavap, and the resulting lipid film was resuspended in 1 ml Buffer L (50 mM Tris-HCl, pH 7.4, 50 mM NaCl) by vigorous vortexing and sonication, yielding a 10 mM lipid suspension. Liposomes with an average diameter of ∼100 nm were obtained by sequential extrusion of the lipid suspension through 0.4-µm, 0.2-µm and 0.1-µm track-etched polycarbonate membranes (Whatman-Nuclepore) and stored under $N_2$ at 4°C until use. Post-nuclear supernatants that had been prepared from HeLa cells transfected with FLAG-tagged CERT, mitoCERT or mitoCERTΔSTART were centrifuged at 100,000 $g_{max}$ for 1 h at 4°C to generate a cytosolic and total membrane fraction. The cytosolic fraction was concentrated using an Amicon Ultra filter unit (nominal molecular mass limit, 10 kDa; MilliPore). Protein concentrations in both fractions were determined by Bradford assay and adjusted to 1 mg/ml in IM Buffer. Cytosolic and membrane fractions were mixed with pacCer-containing liposomes at 1:1 (v:v). Cytosolic fractions were incubated for 30 min at 37°C, and membrane fractions were incubated in the presence of 1 mM β-cyclodextrin for 90 min at 37°C in a thermomixer before UV irradiation for 90 s on ice. UV irradiation was performed using a 1000 W high-pressure mercury lamp (Oriel Photomax) equipped with a Pyrex glass filter to remove wavelengths below 350 nm at a distance of 30 cm from the light source. Samples were subjected to $CHCl_3$:MeOH precipitation, and the resulting protein pellets were resuspended in PBS with 1% SDS for 10 min at 37°C in a thermomixer. Click reactions were performed by incubating ∼20 µg of total protein per sample in 25 µl PBS with 1% SDS containing 1 mM Tris(2-carboxyethyl)phosphin (TCEP), 0.1 mM Tris[(1-benzyl-1H-1,2,3-triazol-4-yl)methyl]amin (TBTA), 1 mM $CuSO_4$ and 80 µM Alexa-Fluor-647 azide for 1 h at 37°C. Next, 5× sample buffer [300 mM Tris, pH 6.8, 10% (w/v) SDS, 50% (v/v) glycerol, 10% (v/v) β-mercaptoethanol and 0.025% (w/v) bromophenol blue] was added, and samples were heated to 95°C for 5 min before SDS-PAGE separation. The gel was washed in milliQ $H_2O$ for 1 h at room temperature, subjected to in-gel fluorescence analysis using a FLA-9500 Biomolecular Imager (GE Healthcare Life Sciences) and then processed for immunoblotting using an anti-FLAG antibody.

### Immunofluorescence microscopy

HeLa cells that had been grown on glass coverslips and transfected as above were fixed in 4% paraformaldehyde in PBS for 10 min, washed in PBS and then quenched in 50 mM $NH_4Cl$ in PBS for 10 min at room temperature. Cells were permeabilized in PM buffer (0.1% saponin and 0.2% BSA in PBS), immuno-labeled with primary antibodies and Cy3- or Cy5-conjugated secondary antibodies, counter stained with DAPI (300 nM in PBS) and mounted in Prolong Gold Antifade Mountant (Thermo Fischer Scientific). Images presented in Figs 2A and 6C were captured at room temperature with a Leica DM5500 B microscope using a 63×1.40 NA Plan Apo oil objective and a SPOT Pursuit camera. Fluorochromes used were DAPI, $\lambda_{excitation}$=360 nm and $\lambda_{emission}$=460 nm; FITC and Alexa-Fluor-488, $\lambda_{excitation}$=488 nm and $\lambda_{emission}$=515 nm; Texas Red and Alexa-Fluor-568, $\lambda_{excitation}$=568 nm and $\lambda_{emission}$=585 nm. Images presented in Fig. 2B were captured at room temperature with an Olympus IX-71 inverted microscope using a 60×1.42 NA Plan ApoN U1S2 objective, a sCMOS camera (PCO, Kelheim, Germany), an InsightSSI illumination system and SoftWoRx 6.0, beta27 software (Applied Precision, Issaquah, WA). Fluorochromes used were DAPI, $\lambda_{excitation}$=390 nm and $\lambda_{emission}$=435 nm; FITC/GFP, $\lambda_{excitation}$=475 nm and $\lambda_{emission}$=523 nm; mCherry/TRITC, $\lambda_{excitation}$=542 nm and $\lambda_{emission}$=594/45 nm; Cy5, $\lambda_{excitation}$=632 nm, $\lambda_{excitation}$=676 nm. Images were processed using Fiji software (NIH, Bethesda, MD).

### *In vivo* ceramide transfer assay

CHO-LYA cells that had been grown on glass cover slips were co-transfected with FLAG-tagged CERT, mitoCERT or mitoCERTΔSTART

and Tom20–GFP. At 24 h post transfection, cells were labeled with 0.5 µM Bodipy–Cer complexed to BSA at 4°C for 20 min and then washed twice in ice-cold Hanks' buffered saline solution (HBSS). After shifting the cells to fresh culture medium, the temperature was raised to 37°C, and fluorescent images were captured at various time points with an Olympus LSM FV1000 confocal microscope using an UPLSAPO 60×1.35 NA oil objective. Fluorochromes used were eGFP, $\lambda_{excitation}$=488 nm and $\lambda_{emission}$=515 nm; Bodipy–Texas-Red, $\lambda_{excitation}$=589 nm and $\lambda_{emission}$=617 nm. Images were processed using Fiji software.

### Super-resolution microscopy

Cells that had been transfected with various DNA constructs were seeded onto glass cover slips coated with poly-L-lysine-polyethylenglucol-arginine-glycine-aspartate (PLL-PEG-RGD) (VandeVondele et al., 2003) 24 h post-transfection and cultured in medium without Phenol Red and with 10 mM HEPES [4-(2-hydroxyethyl)-1-piperazine ethanesulfonic acid]. Cells expressing Halo-tagged proteins were labeled with 30 nM HTL-tetramethylrhodamine (HTL-TMR) (Los and Wood, 2007), washed three times with PBS and then incubated for 1 h in Phenol-Red-free medium with 10 mM HEPES. Cells were processed for immunofluorescence microscopy as described above, but DAPI staining was omitted. Super-resolution microscopy was performed at room temperature using PBS complemented with an oxygen scavenger (0.5 mg/ml glucose oxidase, 40 mg/ml catalase, 5% w/v glucose, 50 mM β-mercaptoethanolamine) to switch the synthetic fluorophores between the on and off states (van de Linde et al., 2012). Imaging was performed with an inverted Olympus IX71 microscope equipped with a Quad-line TIR-illumination condenser, a back-illuminated electron multiplied CCD camera (iXon DU897D, 512×512 pixels from Andor Technology) and a UAPON 150×1.45 NA total internal reflection fluorescence microscope objective. Solid 488-nm (LuxX Omicron), 561-nm (Colbolt Jive) and 647-nm (LuxX Omicron) lasers were coupled into the microscope through a polarization-maintaining monomode fiber (KineFlex, Pointsource). The excitation beam was reflected into the objective by a quad-line dichroic beam splitter for reflection at 405 nm, 488 nm, 568 nm and 647 nm (Di01 R405, 488, 561 and 647, respectively, Semrock). Fluorescence was detected through a quadruple bandpass filter (FF01446, 523, 600 and 677–25, respectively, Semrock).

Images were split by a quadview filter to separate Cy5 and TMR. Fluorescence imaging was performed by excitation at 561 and 647 nm with a typical power density of 1–10 kW/mm$^2$ at the objective. The camera was operated at −80°C with a typical electron-multiplying gain of 300 and a frame rate of 32 Hz. The laser was pulse-synchronized to the camera read-out using the acousto-optic tunable filter and the modulation input of the laser. Localization of each single molecule was achieved using MATLAB based on a modified multiple target algorithm (Sergé et al., 2008). Overlaying the images from different channels with sub-pixel precision was achieved by employing calibration with multicolor fluorescence beads (TetraSpeck microspheres 0.1 µm from Invitrogen) and calculation of a spatial transformation matrix in MATLAB using the function cp2tform and the parameter 'nonreflective similarity'. Pearson colocalization coefficients for ER- and mitochondria-resident fluorescent proteins were determined using the Fiji plugin Coloc 2 (Dunn et al., 2011). The maximum colocalization coefficient, which was observed in rapamycin-treated cells co-expressing HALO-FRB-ER and OMM-FKBP-paGFP, was set at 1. Pearson coefficients were calculated based on duplicate measurements in three independent experiments, using six cells per experimental condition. A two-tailed unpaired Student's *t*-test was performed to determine differences between two groups. Significance was judged when $P<0.05$.

#### Acknowledgements

We thank Karin Busch (University of Osnabrück, Osnabrück, Germany), György Hajnóczky (Thomas Jefferson University, Philadelphia), Toon de Kroon (University of Utrecht, Utrecht, The Netherlands), Neale Ridgway (Dalhousie University, Halifax, Canada) and Richard Youle (National Institute of Health, Bethesda, MD) for sharing DNA constructs and cell lines.

#### Competing interests

The authors declare no competing or financial interests.

#### Author contributions

J.C.M.H. conceived and managed the project. A.J. designed and performed most experiments with crucial input from O.B. and K.E. S.K. synthesized chemical reagents. A.J. and J.C.M.H. wrote the manuscript with hypothesis development, experimental design and data interpretation contributed by all authors.

#### Funding

This work was supported by the European Union Seventh Framework Programme Marie-Curie Innovative Training Networks (ITN) 'Sphingonet' (289278); and the Deutsche Forschungsgemeinschaft Sonderforschungsbereich (SFB944-P14 to J.C.M.H.).

#### References

**Alphonse, G., Bionda, C., Aloy, M.-T., Ardail, D., Rousson, R. and Rodriguez-Lafrasse, C.** (2004). Overcoming resistance to gamma-rays in squamous carcinoma cells by poly-drug elevation of ceramide levels. *Oncogene* **23**, 2703-2715.

**Beverly, L. J., Howell, L. A., Hernandez-Corbacho, M., Casson, L., Chipuk, J. E. and Siskind, L. J.** (2013). BAK activation is necessary and sufficient to drive ceramide synthase-dependent ceramide accumulation following inhibition of BCL2-like proteins. *Biochem. J.* **452**, 111-119.

**Birbes, H., El Bawab, S., Hannun, Y. A. and Obeid, L. M.** (2001). Selective hydrolysis of a mitochondrial pool of sphingomyelin induces apoptosis. *FASEB J.* **15**, 2669-2679.

**Birbes, H., Luberto, C., Hsu, Y.-T., El Bawab, S., Hannun, Y. A. and Obeid, L. M.** (2005). A mitochondrial pool of sphingomyelin is involved in TNFalpha-induced Bax translocation to mitochondria. *Biochem. J.* **386**, 445-451.

**Bose, R., Verheij, M., Haimovitz-Friedman, A., Scotto, K., Fuks, Z. and Kolesnick, R.** (1995). Ceramide synthase mediates daunorubicin-induced apoptosis: an alternative mechanism for generating death signals. *Cell* **82**, 405-414.

**Bourbon, N. A., Sandirasegarane, L. and Kester, M.** (2002). Ceramide-induced inhibition of Akt is mediated through protein kinase Czeta: implications for growth arrest. *J. Biol. Chem.* **277**, 3286-3292.

**Chang, K.-T., Anishkin, A., Patwardhan, G. A., Beverly, L. J., Siskind, L. J. and Colombini, M.** (2015). Ceramide channels: destabilization by Bcl-xL and role in apoptosis. *Biochim. Biophys. Acta* **1848**, 2374-2384.

**Chipuk, J. E., McStay, G. P., Bharti, A., Kuwana, T., Clarke, C. J., Siskind, L. J., Obeid, L. M. and Green, D. R.** (2012). Sphingolipid metabolism cooperates with BAK and BAX to promote the mitochondrial pathway of apoptosis. *Cell* **148**, 988-1000.

**Colombini, M.** (2016). Ceramide channels and mitochondrial outer membrane permeability. *J. Bioenerg. Biomembr.* [Epub ahead of print] doi: 0.1007/s10863-016-9646-z.

**Csordás, G., Renken, C., Várnai, P., Walter, L., Weaver, D., Buttle, K. F., Balla, T., Mannella, C. A. and Hajnóczky, G.** (2006). Structural and functional features and significance of the physical linkage between ER and mitochondria. *J. Cell Biol.* **174**, 915-921.

**Csordás, G., Várnai, P., Golenár, T., Roy, S., Purkins, G., Schneider, T. G., Balla, T. and Hajnóczky, G.** (2010). Imaging interorganelle contacts and local calcium dynamics at the ER-mitochondrial interface. *Mol. Cell* **39**, 121-132.

**Czabotar, P. E., Lessene, G., Strasser, A. and Adams, J. M.** (2014). Control of apoptosis by the BCL-2 protein family: implications for physiology and therapy. *Nat. Rev. Mol. Cell Biol.* **15**, 49-63.

**Dbaibo, G. S., El-Assaad, W., Krikorian, A., Liu, B., Diab, K., Idriss, N. Z., El-Sabban, M., Driscoll, T. A., Perry, D. K. and Hannun, Y. A.** (2001). Ceramide generation by two distinct pathways in tumor necrosis factor alpha-induced cell death. *FEBS Lett.* **503**, 7-12.

**Deng, X., Yin, X., Allan, R., Lu, D. D., Maurer, C. W., Haimovitz-Friedman, A., Fuks, Z., Shaham, S. and Kolesnick, R.** (2008). Ceramide biogenesis is required for radiation-induced apoptosis in the germ line of C. elegans. *Science* **322**, 110-115.

**Dobrowsky, R. T., Kamibayashi, C., Mumby, M. C. and Hannun, Y. A.** (1993). Ceramide activates heterotrimeric protein phosphatase 2A. *J. Biol. Chem.* **268**, 15523-15530.

**Dunn, K. W., Kamocka, M. M. and McDonald, J. H.** (2011). A practical guide to evaluating colocalization in biological microscopy. *Am. J. Physiol. Cell Physiol.* **300**, C723-C742.

**Ďuriš, A., Wiesenganger, T., Moravčíková, D., Baran, P., Kožíšek, J., Daïch, A. and Berkeš, D.** (2011). Expedient and practical synthesis of CERT-dependent ceramide trafficking inhibitor HPA-12 and its analogues. *Org. Lett.* **13**, 1642-1645.

**Ganesan, V., Perera, M. N., Colombini, D., Datskovskiy, D., Chadha, K. and Colombini, M.** (2010). Ceramide and activated Bax act synergistically to permeabilize the mitochondrial outer membrane. *Apoptosis* **15**, 553-562.

**García-Ruiz, C., Colell, A., Marí, M., Morales, A., Calvo, M., Enrich, C. and Fernández-Checa, J. C.** (2003). Defective TNF-alpha–mediated hepatocellular apoptosis and liver damage in acidic sphingomyelinase knockout mice. *J. Clin. Invest.* **111**, 197-208.

**Haberkant, P., Raijmakers, R., Wildwater, M., Sachsenheimer, T., Brügger, B., Maeda, K., Houweling, M., Gavin, A.-C., Schultz, C., van Meer, G. et al.** (2013). In vivo profiling and visualization of cellular protein-lipid interactions using bifunctional fatty acids. *Angew. Chem. Int. Ed. Engl.* **52**, 4033-4038.

**Hait, N. C., Oskeritzian, C. A., Paugh, S. W., Milstien, S. and Spiegel, S.** (2006). Sphingosine kinases, sphingosine 1-phosphate, apoptosis and diseases. *Biochim. Biophys. Acta* **1758**, 2016-2026.

**Hanada, K., Kumagai, K., Yasuda, S., Miura, Y., Kawano, M., Fukasawa, M. and Nishijima, M.** (2003). Molecular machinery for non-vesicular trafficking of ceramide. *Nature* **426**, 803-809.

**Hannun, Y. A. and Obeid, L. M.** (2008). Principles of bioactive lipid signalling: lessons from sphingolipids. *Nat. Rev. Mol. Cell Biol.* **9**, 139-150.

**Huitema, K., van den Dikkenberg, J., Brouwers, J. F. H. M. and Holthuis, J. C. M.** (2004). Identification of a family of animal sphingomyelin synthases. *EMBO J.* **23**, 33-44.

**Kawano, M., Kumagai, K., Nishijima, M. and Hanada, K.** (2006). Efficient trafficking of ceramide from the endoplasmic reticulum to the Golgi apparatus requires a VAMP-associated protein-interacting FFAT motif of CERT. *J. Biol. Chem.* **281**, 30279-30288.

**Kudo, N., Kumagai, K., Matsubara, R., Kobayashi, S., Hanada, K., Wakatsuki, S. and Kato, R.** (2010). Crystal structures of the CERT START domain with inhibitors provide insights into the mechanism of ceramide transfer. *J. Mol. Biol.* **396**, 245-251.

**Kumagai, K., Yasuda, S., Okemoto, K., Nishijima, M., Kobayashi, S. and Hanada, K.** (2005). CERT mediates intermembrane transfer of various molecular species of ceramides. *J. Biol. Chem.* **280**, 6488-6495.

**Kuwana, T., Mackey, M. R., Perkins, G., Ellisman, M. H., Latterich, M., Schneiter, R., Green, D. R. and Newmeyer, D. D.** (2002). Bid, Bax, and lipids cooperate to form supramolecular openings in the outer mitochondrial membrane. *Cell* **111**, 331-342.

**Lee, H., Rotolo, J. A., Mesicek, J., Penate-Medina, T., Rimner, A., Liao, W.-C., Yin, X., Ragupathi, G., Ehleiter, D., Gulbins, E. et al.** (2011). Mitochondrial ceramide-rich macrodomains functionalize Bax upon irradiation. *PLoS ONE* **6**, e19783.

**Liu, Z., Xia, Y., Li, B., Xu, H., Wang, C., Liu, Y., Li, Y., Li, C., Gao, N. and Li, L.** (2014). Induction of ER stress-mediated apoptosis by ceramide via disruption of ER Ca(2+) homeostasis in human adenoid cystic carcinoma cells. *Cell Biosci.* **4**, 71.

**Loewen, C. J. R., Roy, A. and Levine, T. P.** (2003). A conserved ER targeting motif in three families of lipid binding proteins and in Opi1p binds VAP. *EMBO J.* **22**, 2025-2035.

**Los, G. V. and Wood, K.** (2007). The HaloTag: a novel technology for cell imaging and protein analysis. *Methods Mol. Biol.* **356**, 195-208.

**Luberto, C., Hassler, D. F., Signorelli, P., Okamoto, Y., Sawai, H., Boros, E., Hazen-Martin, D. J., Obeid, L. M., Hannun, Y. A. and Smith, G. K.** (2002). Inhibition of tumor necrosis factor-induced cell death in MCF7 by a novel inhibitor of neutral sphingomyelinase. *J. Biol. Chem.* **277**, 41128-41139.

**Luna-Vargas, M. P. A. and Chipuk, J. E.** (2016). The deadly landscape of pro-apoptotic BCL-2 proteins in the outer mitochondrial membrane. *FEBS J.* **283**, 2676-2689.

**Mesicek, J., Lee, H., Feldman, T., Jiang, X., Skobeleva, A., Berdyshev, E. V., Haimovitz-Friedman, A., Fuks, Z. and Kolesnick, R.** (2010). Ceramide synthases 2, 5, and 6 confer distinct roles in radiation-induced apoptosis in HeLa cells. *Cell. Signal.* **22**, 1300-1307.

**Moldoveanu, T., Follis, A. V., Kriwacki, R. W. and Green, D. R.** (2014). Many players in BCL-2 family affairs. *Trends Biochem. Sci.* **39**, 101-111.

**Mukhopadhyay, A., Saddoughi, S. A., Song, P., Sultan, I., Ponnusamy, S., Senkal, C. E., Snook, C. F., Arnold, H. K., Sears, R. C., Hannun, Y. A. et al.** (2009). Direct interaction between the inhibitor 2 and ceramide via sphingolipid-protein binding is involved in the regulation of protein phosphatase 2A activity and signaling. *FASEB J.* **23**, 751-763.

**Park, M. A., Zhang, G., Martin, A. P., Hamed, H., Mitchell, C., Hylemon, P. B., Graf, M., Rahmani, M., Ryan, K., Liu, X. et al.** (2008). Vorinostat and sorafenib increase ER stress, autophagy and apoptosis via ceramide-dependent CD95 and PERK activation. *Cancer Biol. Ther.* **7**, 1648-1662.

**Patwardhan, G. A., Beverly, L. J. and Siskind, L. J.** (2016). Sphingolipids and mitochondrial apoptosis. *J. Bioenerg. Biomembr.* **48**, 153-168.

**Renault, T. T., Floros, K. V., Elkholi, R., Corrigan, K.-A., Kushnareva, Y., Wieder, S. Y., Lindtner, C., Serasinghe, M. N., Asciolla, J. J., Buettner, C. et al.** (2015). Mitochondrial shape governs BAX-induced membrane permeabilization and apoptosis. *Mol. Cell* **57**, 69-82.

**Salvador-Gallego, R., Mund, M., Cosentino, K., Schneider, J., Unsay, J., Schraermeyer, U., Engelhardt, J., Ries, J. and García-Sáez, A. J.** (2016). Bax assembly into rings and arcs in apoptotic mitochondria is linked to membrane pores. *EMBO J.* **35**, 389-401.

**Ségui, B., Andrieu-Abadie, N., Jaffrézou, J.-P., Benoist, H. and Levade, T.** (2006). Sphingolipids as modulators of cancer cell death: potential therapeutic targets. *Biochim. Biophys. Acta* **1758**, 2104-2120.

**Senkal, C. E., Ponnusamy, S., Manevich, Y., Meyers-Needham, M., Saddoughi, S. A., Mukhopadyay, A., Dent, P., Bielawski, J. and Ogretmen, B.** (2011). Alteration of ceramide synthase 6/C16-ceramide induces activating transcription factor 6-mediated Endoplasmic Reticulum (ER) stress and apoptosis via perturbation of cellular Ca2+ and ER/golgi membrane network. *J. Biol. Chem.* **286**, 42446-42458.

**Sergé, A., Bertaux, N., Rigneault, H. and Marguet, D.** (2008). Dynamic multiple-target tracing to probe spatiotemporal cartography of cell membranes. *Nat. Methods* **5**, 687-694.

**Siskind, L. J., Kolesnick, R. N. and Colombini, M.** (2002). Ceramide channels increase the permeability of the mitochondrial outer membrane to small proteins. *J. Biol. Chem.* **277**, 26796-26803.

**Siskind, L. J., Kolesnick, R. N. and Colombini, M.** (2006). Ceramide forms channels in mitochondrial outer membranes at physiologically relevant concentrations. *Mitochondrion* **6**, 118-125.

**Siskind, L. J., Feinstein, L., Yu, T., Davis, J. S., Jones, D., Choi, J., Zuckerman, J. E., Tan, W., Hill, R. B., Hardwick, J. M. et al.** (2008). Anti-apoptotic Bcl-2 Family Proteins Disassemble Ceramide Channels. *J. Biol. Chem.* **283**, 6622-6630.

**Siskind, L. J., Mullen, T. D., Romero Rosales, K., Clarke, C. J., Hernandez-Corbacho, M. J., Edinger, A. L. and Obeid, L. M.** (2010). The BCL-2 protein BAK is required for long-chain ceramide generation during apoptosis. *J. Biol. Chem.* **285**, 11818-11826.

**Stiban, J., Caputo, L. and Colombini, M.** (2008). Ceramide synthesis in the endoplasmic reticulum can permeabilize mitochondria to proapoptotic proteins. *J. Lipid Res.* **49**, 625-634.

**Swanton, C., Marani, M., Pardo, O., Warne, P. H., Kelly, G., Sahai, E., Elustondo, F., Chang, J., Temple, J., Ahmed, A. A. et al.** (2007). Regulators of mitotic arrest and ceramide metabolism are determinants of sensitivity to paclitaxel and other chemotherapeutic drugs. *Cancer Cell* **11**, 498-512.

**Tafesse, F. G., Ternes, P. and Holthuis, J. C. M.** (2006). The multigenic sphingomyelin synthase family. *J. Biol. Chem.* **281**, 29421-29425.

**Tafesse, F. G., Vacaru, A. M., Bosma, E. F., Hermansson, M., Jain, A., Hilderink, A., Somerharju, P. and Holthuis, J. C. M.** (2014). Sphingomyelin synthase-related protein SMSr is a suppressor of ceramide-induced mitochondrial apoptosis. *J. Cell Sci.* **127**, 445-454.

**Tait, S. W. G. and Green, D. R.** (2013). Mitochondrial regulation of cell death. *Cold Spring Harb. Perspect. Biol.* **5**, a008706.

**Tidhar, R. and Futerman, A. H.** (2013). The complexity of sphingolipid biosynthesis in the endoplasmic reticulum. *Biochim. Biophys. Acta* **1833**, 2511-2518.

**Trajkovic, K., Hsu, C., Chiantia, S., Rajendran, L., Wenzel, D., Wieland, F., Schwille, P., Brügger, B. and Simons, M.** (2008). Ceramide triggers budding of exosome vesicles into multivesicular endosomes. *Science* **319**, 1244-1247.

**Vacaru, A. M., Tafesse, F. G., Ternes, P., Kondylis, V., Hermansson, M., Brouwers, J. F. H. M., Somerharju, P., Rabouille, C. and Holthuis, J. C. M.** (2009). Sphingomyelin synthase-related protein SMSr controls ceramide homeostasis in the ER. *J. Cell Biol.* **185**, 1013-1027.

**Vacaru, A. M., van den Dikkenberg, J., Ternes, P. and Holthuis, J. C. M.** (2013). Ceramide phosphoethanolamine biosynthesis in Drosophila is mediated by a unique ethanolamine phosphotransferase in the Golgi lumen. *J. Biol. Chem.* **288**, 11520-11530.

**van de Linde, S., Heilemann, M. and Sauer, M.** (2012). Live-cell super-resolution imaging with synthetic fluorophores. *Annu. Rev. Phys. Chem.* **63**, 519-540.

**VandeVondele, S., Vörös, J. and Hubbell, J. A.** (2003). RGD-grafted poly-L-lysine-graft-(polyethylene glycol) copolymers block non-specific protein adsorption while promoting cell adhesion. *Biotechnol. Bioeng.* **82**, 784-790.

**von Haefen, C., Wieder, T., Gillissen, B., Stärck, L., Graupner, V., Dörken, B. and Daniel, P. T.** (2002). Ceramide induces mitochondrial activation and apoptosis via a Bax-dependent pathway in human carcinoma cells. *Oncogene* **21**, 4009-4019.

**Wang, C. and Youle, R. J.** (2012). Predominant requirement of Bax for apoptosis in HCT116 cells is determined by Mcl-1's inhibitory effect on Bak. *Oncogene* **31**, 3177-3189.

**Wang, X., Rao, R. P., Kosakowska-Cholody, T., Masood, M. A., Southon, E., Zhang, H., Berthet, C., Nagashim, K., Veenstra, T. K., Tessarollo, L. et al.** (2009). Mitochondrial degeneration and not apoptosis is the primary cause of embryonic lethality in ceramide transfer protein mutant mice. *J. Cell Biol.* **184**, 143-158.

**Wei, M. C., Zong, W.-X., Cheng, E. H.-Y., Lindsten, T., Panoutsakopoulou, V., Ross, A. J., Roth, K. A., MacGregor, G. R., Thompson, C. B. and Korsmeyer, S. J.** (2001). Proapoptotic BAX and BAK: a requisite gateway to mitochondrial dysfunction and death. *Science* **292**, 727-730.

**Wilmes, S., Beutel, O., Li, Z., Francois-Newton, V., Richter, C. P., Janning, D., Kroll, C., Hanhart, P., Hötte, K., You, C. et al.** (2015). Receptor dimerization dynamics as a regulatory valve for plasticity of type I interferon signaling. *J. Cell Biol.* **209**, 579-593.

**Yamaoka, S., Miyaji, M., Kitano, T., Umehara, H. and Okazaki, T.** (2004). Expression cloning of a human cDNA restoring sphingomyelin synthesis and cell growth in sphingomyelin synthase-defective lymphoid cells. *J. Biol. Chem.* **279**, 18688-18693.

**Zhu, Q.-Y., Wang, Z., Ji, C., Cheng, L., Yang, Y.-L., Ren, J., Jin, Y.-H., Wang, Q.-J., Gu, X.-J., Bi, Z.-G. et al.** (2011). C6-ceramide synergistically potentiates the anti-tumor effects of histone deacetylase inhibitors via AKT dephosphorylation and α-tubulin hyperacetylation both in vitro and in vivo. *Cell Death Dis.* **2**, e117.